ACS NANOSCIENCE Au
AN OPEN ACCESS JOURNAL OF THE AMERICAN CHEMICAL SOCIETY

pubs.acs.org/nanoau Article

Efficient Preparation of a Magnetic Helical Carbon Nanomotor for Targeted Anticancer Drug Delivery

Yanming Sun, Renjie Pan, Yuduo Chen, Yong Wang, Lei Sun, Neng Wang, Xing Ma,* and Guo Ping Wang*

Cite This: *ACS Nanosci. Au* 2023, 3, 94–102 Read Online

ACCESS | Metrics & More | Article Recommendations | Supporting Information

ABSTRACT: The applications of nanomotors in the biomedical field have been attracting extensive attention. However, it remains a challenge to fabricate nanomotors in a facile way and effectively load drugs for active targeted therapy. In this work, we combine the microwave heating method and chemical vapor deposition (CVD) to fabricate magnetic helical nanomotors efficiently. The microwave heating method can accelerate intermolecular movement, which converts kinetic energy into heat energy and shortens the preparation time of the catalyst used for carbon nanocoil (CNC) synthesis by 15 times. Fe_3O_4 nanoparticles are in situ nucleated on the CNC surface by the microwave heating method to fabricate magnetically driven CNC/Fe_3O_4 nanomotors. In addition, we achieved precise control of the magnetically driven CNC/Fe_3O_4 nanomotors through remote manipulation of magnetic fields. Anticancer drug doxorubicin (DOX) is then efficiently loaded onto the nanomotors via $\pi-\pi$ stacking interactions. Finally, the drug-loaded CNC/Fe_3O_4@DOX nanomotor can accurately accomplish cell targeting under external magnetic field control. Under short-time irradiation of near-infrared light, DOX can be quickly released onto target cells to effectively kill the cells. More importantly, CNC/Fe_3O_4@DOX nanomotors allow for single-cell or cell-cluster-targeted anticancer drug delivery, providing a dexterous platform to potentially perform many medically relevant tasks in vivo. The efficient preparation method and application in drug delivery are beneficial for future industrial production and provide inspiration for advanced micro/nanorobotic systems using the CNC as a carrier for a wide range of biomedical applications.

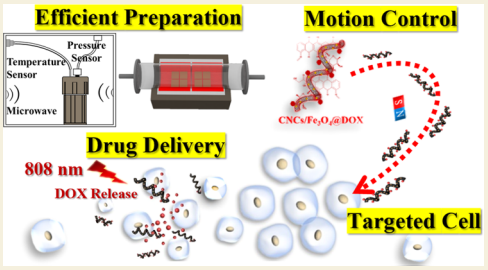

KEYWORDS: *carbon helix, magnetic nanomotors, helical structure, magnetic control, targeted drug delivery*

INTRODUCTION

So far, surgical treatment,[1−3] chemotherapy,[4−6] and radiotherapy[7−9] are still the main means of clinical tumor treatment, but these traditional therapies cannot effectively eradicate cancer because of lacking the ability to precisely target cancer cells.[10] Therefore, there are high expectations for micro/nanomachines that can target cells.[11] Spontaneous reactions on site or external fields are needed to provide a driving force for the movement of these tiny machines, such as nanoswimmers,[12−14] nanorockets,[15,16] Janus nanomotors,[17−19] and biologically inspired microbots.[20] The micro/nanomotors are of great potential in biological medicine, including analytical sensing,[21,22] drug delivery,[23−25] nanosurgery,[26] and bioimaging.[27] Especially in drug delivery, micro/nanomotors have been widely reported to be used for loading, carrying, and transporting chemotherapy drugs.[28] However, the biocompatibility, drug loading, and drug release efficiency of these micro/nanomotors are still important issues that need to be solved in the field of biomedicine.

Many types of materials have been used to fabricate micro/nanomotors, such as TiO_2,[29,30] MOF[31] (metal−organic frameworks), graphene, and its allotropes.[32,33] These materials are often modified by metallic components or contain toxic substances, which may cause irreversible damage to the biological systems when used in biomedicine. For the different driving modes of micro/nanomotors, many strategies have been tried.[34] The chemical fuel-driven micro/nanomotors mainly use hydrogen peroxide as chemical fuel, which is toxic and may affect the stability of biological receptors and biometric recognition problems when applied to organisms.[17,35,36] Light-driven micro/nanomotors are mainly based on the use of the asymmetric structure of the nanomotor and the gradient change of the optical field to drive the motion of nanomotors. The light source usually adopts high-intensity ultraviolet light or infrared light. Prolonged high-intensity exposure to such light sources can cause irreversible damage to the nanomotor's body itself.[30,37] Therefore, the application of nanomaterials with good biocompatibility combined with clean, nontoxic, and

Received: August 30, 2022
Revised: November 4, 2022
Accepted: November 8, 2022
Published: November 25, 2022

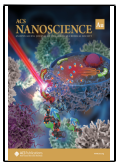

https://doi.org/10.1021/acsnanoscienceau.2c00042
ACS Nanosci. Au 2023, 3, 94–102

Scheme 1. Schematic Diagram of the Fabrication of Functionalized CNC/Fe_3O_4@DOX Nanomotors Targeting HeLa Cells and Laser-Induced DOX Drug Delivery for Cancer Cell Therapy

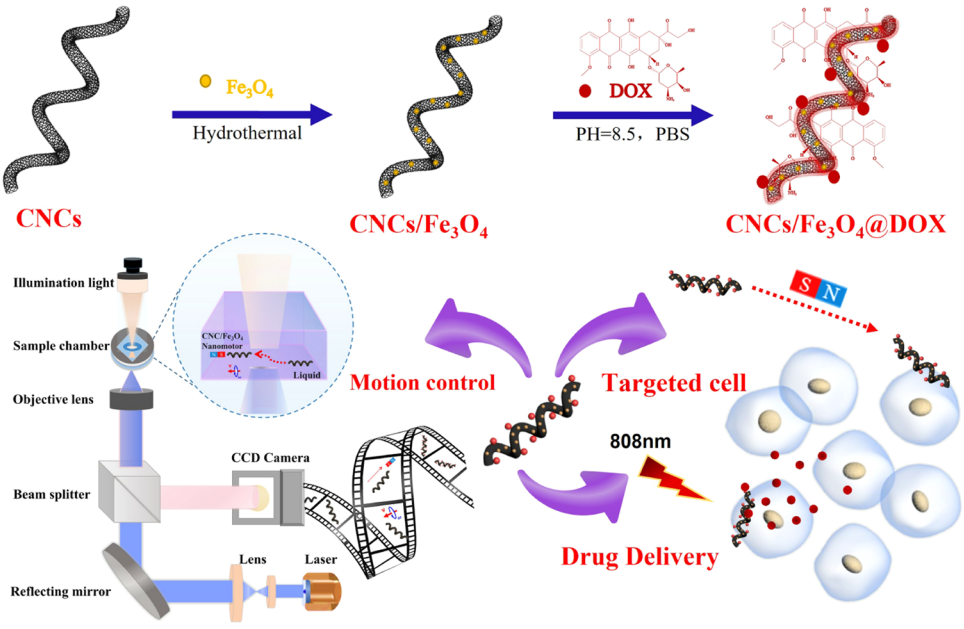

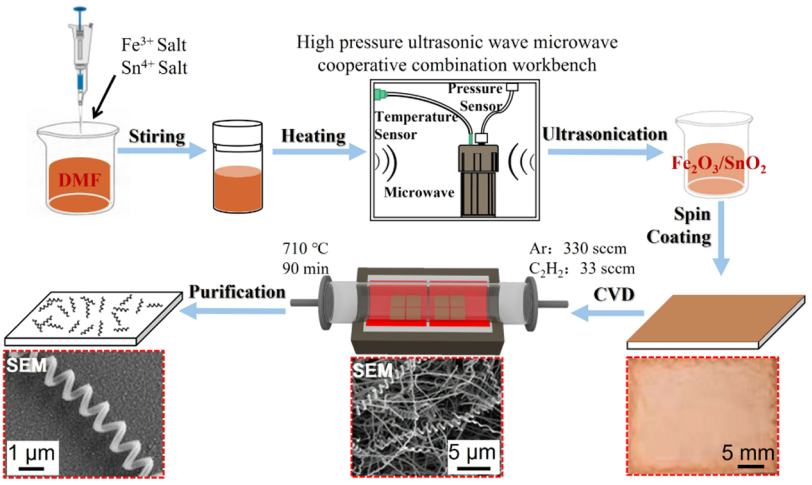

Figure 1. Flow chart of CNC preparation by the microwave heating method.

efficient driving methods is particularly important for applications in the biomedical field.[38]

Carbon nanocoils (CNCs) are based on carbon materials with helical structures, good biocompatibility, unique conjugated structure, and a large specific surface area.[39] The $\pi-\pi$ bonds on the surface of CNCs are easy for functional modifications. In the field of magnetic nanoparticles, various types of iron oxides (mainly maghemite, γ-Fe_2O_3, or magnetite, Fe_3O_4)[40,41] have been increasingly investigated. Magnetite Fe_3O_4 is a very promising option as a common magnetic iron oxide because of its proven biocompatibility.[42,43] The motion control of the CNCs decorated with Fe_3O_4 nanoparticles can be performed under the action of an external magnetic field. The motion of nanomotors driven by an external magnetic field is a method commonly used in the field of biomedicine. It does not require chemical substances and can be remotely controlled by changing the parameters related to the magnetic field to realize the directional movement of magnetic substances. The remote control of external magnetic fields is especially advantageous for remote control in closed systems.

In this work, we propose a magnetically actuated CNC/Fe_3O_4 nanomotor for targeting HeLa cells and laser-induced doxorubicin (DOX) drug delivery for cancer cell therapy (Scheme 1). We innovatively combine the microwave heating method and chemical vapor deposition (CVD) to fabricate magnetic CNC/Fe_3O_4 nanomotors in large quantities. The microwave heating approach efficiently eliminates CNC catalyst agglomeration and is favorable to surface functional modification. The crystallinity and yield of CNCs are significantly influenced by the particle size and distribution of catalyst particles on the substrate. The process of microwave heating can accelerate intermolecular movement, which converts kinetic energy into heat energy and shortens the preparation time of the catalyst used for carbon nanocoil (CNC) synthesis by 15 times. Through the logical design of the catalyst and the efficient integration of the microwave heating method and the CVD process, we achieve the efficient preparation of high-purity

https://doi.org/10.1021/acsnanoscienceau.2c00042
ACS Nanosci. Au 2023, 3, 94−102

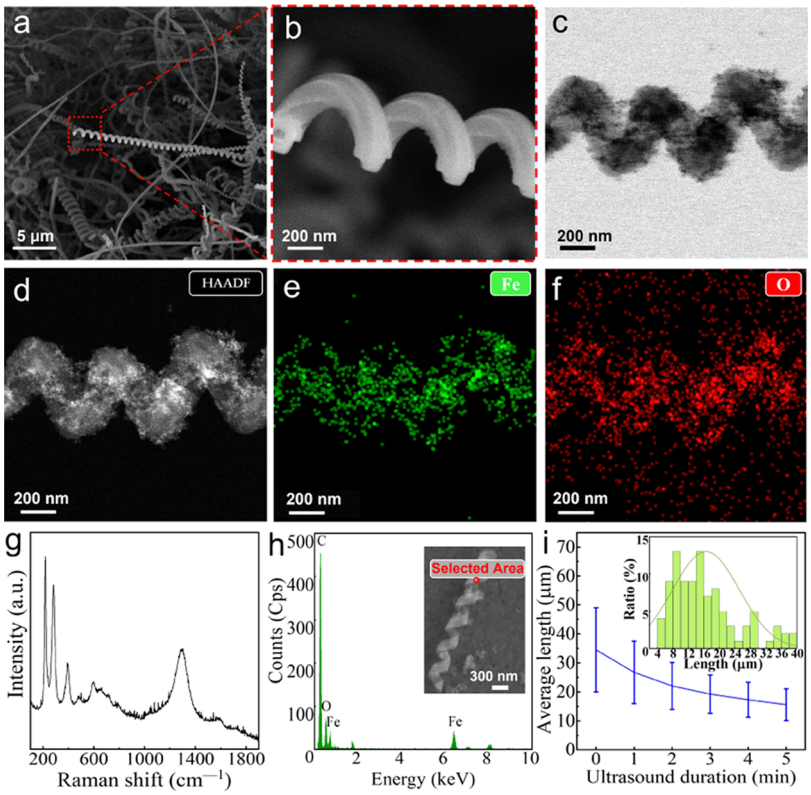

Figure 2. (a) SEM image of CNCs, (b) SEM enlarged image of the partial CNC, (c) BF (bright field) image of CNC/Fe_3O_4 nanomotors, (d) HAADF of CNC/Fe_3O_4 nanomotors, (e) TEM-EDS elemental mapping of Fe elements in CNC/Fe_3O_4 nanomotors, (f) TEM-EDS elemental mapping of O elements in CNC/Fe_3O_4 nanomotors, (g) Raman shift of the CNC/Fe_3O_4 nanomotors, (h) SEM-EDS spectrum of the CNC/Fe_3O_4 nanomotors, and (i) average length of the CNCs with different ultrasound breaking durations.

CNCs. CNCs can be well modified with magnetic Fe_3O_4 nanoparticles and load DOX through $\pi-\pi$ stacking. The nanomotors were activated by applying an external direct current (DC) or a rotating magnetic field for motion control along any predesigned path. Then, the CNC/Fe_3O_4 nanomotors are loaded with DOX to prepare CNC/Fe_3O_4@DOX nanomotors for remote manipulation to actively target cancer cells. Based on the good response and absorption characteristics of CNCs to near-infrared light, the functionalized CNC/Fe_3O_4@DOX nanomotors can effectively release DOX under short-term (~180 s) irradiation of near-infrared light. The results show that the CNC/Fe_3O_4@DOX nanomotor has a good ability to target cells under the action of an external magnetic field and can effectively release DOX on the target cells to enhance localized concentrations, thereby effectively killing the target cells. The efficient preparation of this helical carbon-based nanomotor and its innovative application in drug delivery lays the foundation for the application of CNC-based nanomotors in biomedicine and also provides inspiration for the design and preparation of new intelligent artificial micro/nanomotors.

EXPERIMENTAL SECTION

The preparation process of CNCs is shown in Figure 1. First, a Fe/Sn catalyst was synthesized by the microwave heating method. Then, CNCs were prepared by CVD. The details of each step of CNC preparation and CNC/Fe_3O_4@DOX nanomotor synthesis were as follows:

Preparation of the Fe/Sn Catalyst

First, 0.5 mmol soluble Fe^{3+} salt was dissolved in (30 mL) *N*,*N*-dimethylformamide (DMF).[44] Then, 0.05 mmol soluble Sn^{4+} salt was added to the mixed solution with a molar ratio of Fe^{3+} to Sn^{4+} of 10:1. After 30 min of ultrasound, the mixture was transferred to a 100 mL Teflon container. It was transferred to the high-pressure ultrasonic-microwave cooperative combination workstation and heated by a microwave at 160 w and 150 °C for 120 min. Finally, the catalyst solution was filtered and collected by vacuum filtration with a cellulose membrane with a pore size of 0.22 (μm). A Fe−Sn catalyst ethanol dispersion was prepared at a concentration of 1 mg mL^{-1}, and ultrasonication was conducted for 3 h until it was uniform and ready for use.

Preparation of CNCs

A catalyst-coated Al_2O_3 substrate was placed in a CVD system, and argon gas was injected into the reaction tube at a flow rate of 660 sccm. When the furnace was heated to 710 °C, 35 sccm C_2H_2 gas was injected, and the reaction was kept for 3 h. The reaction time determines the size of the grown CNC samples. After the reaction, acetylene gas was turned off, and the CVD system was cooled to room temperature under argon protective gas. Finally, argon gas and the CVD system were turned off. The samples were removed from the tube furnace, and the tubes were cleaned at 710 °C for 1 h.

Synthesis of the CNC/Fe_3O_4 Nanomotors

CNC/Fe_3O_4 nanomotors were synthesized by the microwave heating method. First, 200 mg of CNCs was dispersed in 68 wt % nitric acid and acidified for 1 h. Then, the CNCs were filtered and dispersed in deionized water for 1 h. After sonication for 5 min, 150 mL of deionized water was added to the filtered CNCs, followed by 100 mg of $FeSO_4 \cdot 7H_2O$, 2000 mg of $FeCl_3 \cdot 6H_2O$, 500 mg of poly(ethylene glycol) 20 000, and 0.5 mL of ammonia. The mixed solution was stirred well and transferred to a 100 mL poly(tetrafluoroethylene) container. The microwave power was 160 W, and the temperature was set to 150 °C for 1 h. Finally, the solution was centrifuged at 5000 rpm for 10 min.

https://doi.org/10.1021/acsnanoscienceau.2c00042
ACS Nanosci. Au 2023, 3, 94−102

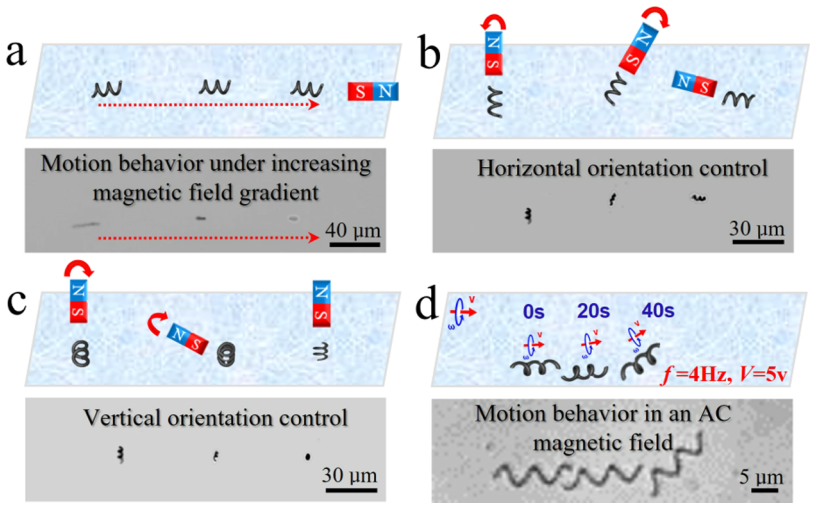

Figure 3. Scheme and experimental results of nanomotors under magnetic field control. (a) Linear motion (Video S1, Supporting Information), (b) horizontal direction control (Video S2, Supporting Information), (c) vertical direction control (Video S3, Supporting Information), and (d) motion behavior in an AC magnetic field (Video S4, Supporting Information).

Synthesis of the CNC/Fe_3O_4@DOX Nanomotors

The unique helical morphology of CNCs has a large specific surface area, and the conjugated structure of carbon nanomaterials exhibits excellent physical and chemical properties, which are suitable for $\pi-\pi$ stacking interactions with many drugs and therapeutic molecules with aromatic rings, including anthracyclines. DOX is a typical anthracycline anticancer agent that can be easily adsorbed on the surface of CNCs by $\pi-\pi$ stacking.[45] First, we pipetted out 2 mL of pH = 7 phosphate-buffered saline (PBS). Then, tris(hydroxymethyl)aminomethane standard buffer was added to PBS to adjust its pH to 8.5. Next, 0.1 mmol DOX and 0.1 mg of CNC/Fe_3O_4 nanomotors were added to PBS at pH 8.5 and stirred for 10 min before being refrigerated at 4 °C for 2 days. Finally, the solution was separated by centrifugation at 6000 rpm for 30 min.

Characterization

The CNCs were mainly synthesized by the CVD system model GSL-5Z-LCD produced by Hefei Kejing Materials Technology Co. The Sn/Fe catalyst and the CNC/Fe_3O_4 nanomotor were prepared using a high-pressure ultrasonic-microwave synergistic workbench model XH-300PE produced by Beijing Xianghu Technology Development Co. The Raman spectra patterns of the samples were obtained by a Raman spectrometer under laser excitation at 633 nm. The samples were characterized using a Supra 55 Sapphire field-emission scanning electron microscope (SEM) (Germany) and energy-dispersive X-ray spectroscopy (EDS) analysis. High-resolution TEM (HRTEM) images were obtained using a JEOL 2200FS electron microscope operating at 200 kV with an energy-dispersive spectrometer (EDS), an intracolumn energy (Omega) filter, and a high-angle annular dark-field (HAADF) detector.

RESULTS AND DISCUSSION

CNC/Fe_3O_4 nanomotors were synthesized by the microwave heating method and CVD. SEM was used to observe the morphology of the sample, as shown in Figure 2a. CNCs showed a unique geometric spiral morphology. The rough surface of CNCs (enlarged SEM image of part of CNCs, Figure 2b) favors the formation of Fe_3O_4 nanoparticles. It can be observed that after ultrasonic cleaning of CNC/Fe_3O_4 nanomotors, Fe_3O_4 nanoparticles are stably attached to the CNC surface, as shown in Figure 2c (CNC/Fe_3O_4 nanomotor bright-field (BF) image), indicating that Fe_3O_4 nanoparticles are in situ nucleated and attached to the CNCs.[46] To further observe the distribution of Fe_3O_4 nanoparticles on the surface of CNCs, high-resolution transmission electron microscopy (HRTEM) was used in combination with high-angle circular dark-field imaging (HAADF, Figure 2d) and energy-dispersive X-ray spectroscopy (EDS). The C material serves as a skeleton structure, while Fe and O elements are uniformly wrapped around the surface of the CNC (Figure 2e,f). It is clearly seen that the Fe_3O_4 nanoparticles are uniformly distributed on the surface of CNCs. Figure 2g shows the Raman spectrum of CNC/Fe_3O_4 nanomotors. It can be seen from the figure that there is a D band at 1336 cm^{-1} and a G band at 1589 cm^{-1}, which are two characteristic peaks of graphite-like materials. Generally speaking, the D band is caused by structural defects, while the G band is derived from the graphite structure of carbon materials.[29] At the same time, 289 and 403 cm^{-1} correspond to the characteristic peaks of α-Fe_2O_3,[47] 665 and 535 cm^{-1} correspond to Fe_3O_4 characteristic peaks,[48,49] and 1336 and 1589 cm^{-1} correspond to CNC characteristic peaks. In addition, the SEM-EDS spectrum (Figure 2h) shows that CNC/Fe_3O_4 nanomotors are mainly composed of Fe, O, and C, indicating that Fe_3O_4 exists on the surface of CNC. The prepared CNCs were broken up into segments of nanohelices of different lengths with the variation of ultrasound time, as shown in Figure 2i. With an increase in ultrasonication time, the length of CNCs becomes shorter, and the proportion of short CNCs also increases.

The CNC/Fe_3O_4 nanomotors dispersed in an aqueous solution can be motion-controlled by small neodymium–iron–boron (NdFeB) disc magnets by controlling the linear distance and direction between the magnets and the CNC/Fe_3O_4 nanomotors. Due to the induced torque exerted by the DC magnetic field on the CNC/Fe_3O_4 nanomotors, the force direction of each CNC/Fe_3O_4 nanomotor was aligned with the direction of the magnet to match its magnetization direction. Similar to the attraction of a compass in response to a DC magnetic field. If the magnetic field gradient is high enough, it can pull the nanomotor. Thus, we can remotely manipulate the nanomotor to perform different tasks in an aqueous solution with this simple magnetic field. As shown in Figure 3a–c, we controlled the direction, position, and rotation of the CNC/Fe_3O_4 nanomotors in three dimensions. The motion of the nanomotor in the magnetic field was affected by the magnetization of a single CNC/Fe_3O_4 nanomotor, which was

https://doi.org/10.1021/acsnanoscienceau.2c00042
ACS Nanosci. Au 2023, 3, 94–102

determined by the mass of Fe_3O_4, the magnetization of the external magnet, the weight of the CNC, and the dispersion degree of Fe_3O_4 nanoparticles on the CNC surface. In general, the position, direction, and speed of nanomotors can be remotely controlled by the applied magnetic gradient.[50] As shown in Figure 3a, the magnet was first placed in the horizontal direction of the nanomotor position, and the motion direction of the nanomotor was consistent with the direction of the magnetic field and started to move in a straight line along the direction of the magnet. The closer the nanomotor was to the magnet, the faster the nanomotor moved (~12 μm s^{-1}). Next, we controlled to control the distance between the magnet and the nanomotors to keep the nanomotor and the magnet relatively stationary. By rotating the magnet, we observed the rotational motion of the nanomotors in the horizontal plane (as shown in Figure 3b) and the vertical plane (as shown in Figure 3c). Finally, CNC/Fe_3O_4 nanomotors can also be controlled by an alternating current (AC) magnetic field. As shown in Figure 3d, the motion of the CNC/Fe_3O_4 nanomotor in an aqueous solution was realized by controlling the frequency and voltage of the AC magnetic field. The multidimensional motion mode displayed by CNCs/Fe_3O_4 nanomotors in liquids can efficiently overcome the resistance of viscous liquids, hence enabling the realization of rapid motion. In addition, the high specific surface area of the helix facilitates the loading and transport of the drugs. It is advantageous for use in the complicated system of biological cells.

The conjugated structure of CNCs is suitable for modification with drugs and aromatic ring-like drug molecules. DOX is a typical anthracycline anticancer agent that can be adsorbed on the surface of CNC/Fe_3O_4 nanomotors by $\pi-\pi$ stacking. As a fluorescent anticancer drug, DOX can emit red fluorescence under the excitation of a green laser. Figure 4a shows the morphology of the single CNC/Fe_3O_4@DOX nanomotor under an optical microscope.

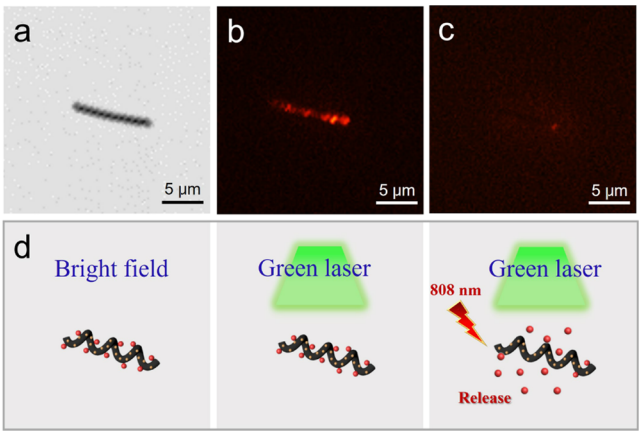

Figure 4. (a) CNC/Fe_3O_4@DOX nanomotor under an optical microscope, (b) fluorescence microscope, and (c) after being irradiated by an 808 nm laser irradiation of a 2 W cm^{-2} power density for 180 s. (d) Schematic diagram of the release process of DOX under the green laser response of the CNC/Fe_3O_4@DOX nanomotor.

As shown in Figure 4b, the CNC was observed to emit red fluorescence under the excitation of a green laser by a fluorescence microscope, and the fluorescence was wrapped on the surface of the CNC. The fluorescence intensity characterizes the carrying degree of DOX. The stronger the fluorescence intensity, the more DOX is modified by the CNC/Fe_3O_4@DOX nanomotor. The red fluorescence on the surface of the CNC/Fe_3O_4 nanomotor started to dissipate under the irradiation of near-infrared light at a wavelength of 808 nm. Finally, the red fluorescence almost disappeared completely after 180 s. The DOX on the CNC/Fe_3O_4@DOX nanomotor was basically released under the excitation of the green laser (as shown in Figure 4c), and the schematic diagram of the process is shown in Figure 4d. It also demonstrates that DOX is successfully adsorbed on the surface of CNC/Fe_3O_4 nanomotors and DOX can be effectively released under near-infrared (NIR) light irradiation.

As shown in Figure 5, a single CNC/Fe_3O_4@DOX nanomotor was successfully moved to the target HeLa cells within 150 s under the remote control of an external magnetic field. Due to the helical structure and the rough surface of the CNC, as well as the grooves on the surface of HeLa cells, CNC/Fe_3O_4@DOX nanomotors can be firmly attached to the surface of HeLa cells. Figure 6 demonstrates the comparison of bright-field images and fluorescence images of CNCs/Fe_3O_4@DOX nanomotors, targeting a single target HeLa cell, and clustered nanomotors, targeting a group of cells before and after NIR irradiation at a wavelength of 808 nm. Figure 6a further confirms that the CNC/Fe_3O_4@DOX nanomotor was successfully attached to the surface of living HeLa cells. In addition, there was one normally dead HeLa cell that fluoresced red, which came from propidium iodide in solution entering the nucleus through a crack in the cell membrane while the rest of the cells were alive (as shown in Figure 6b). After irradiation with an 808 nm NIR laser (2 W cm^{-2}) for 180 s, only the live cells equipped with CNC/Fe_3O_4@DOX nanomotors became dead and showed red fluorescence under fluorescence microscopy (as shown in Figure 6c). It indicates that the CNC/Fe_3O_4@DOX nanomotor successfully released DOX and formed a relatively high concentration in the target area, resulting in the death of the target cells while other living cells remained alive. Figure 6d exhibits the fluorescence contrast graph of a single CNCs/Fe_3O_4@DOX nanomotor targeting a single target HeLa cell. To test the killing ability of DOX drug release of CNC/Fe_3O_4@DOX nanomotors on a large number of cells, we carried out a comparative experiment in which the cell solution mixed with CNC/Fe_3O_4@DOX nanomotors and a pure HeLa cell solution was left standing for the same time. Figure 6e,g demonstrates bright-field images of HeLa cells in mixed solutions containing CNCs/Fe_3O_4@DOX nanomotor clusters and in pure solutions, respectively. The results showed that HeLa cells in the laser-irradiated area died almost completely after 46 min (Figure 6f), while in the control experiments without CNC/Fe_3O_4@DOX nanomotors, only a few HeLa cells were found to die normally (Figure 6h). Schematic diagrams of single targeted drug delivery and clustered drug delivery behavior of CNC/Fe_3O_4@DOX nanomotors are shown in Figure 6i–l, where Figure 6I,j shows individual nanomotors targeting individual HeLa cells and Figure 6k,l shows population nanomotors targeting a group of targeted cells. It demonstrated that the drug-loaded CNCs/Fe_3O_4@DOX nanomotors could perform multiple forms of tasks under different conditions. It also facilitated the functionalized helical nanomotors for nanomedicine applications in complex systems. The aggregation behavior of micronanomotors has the potential for numerous biomedical applications. In complicated biomedical systems, micro–nano groups can offer effective solutions to difficult challenges. This aggregated activity has the potential to advance therapeutic and diagnostic technologies dramatically.[51,52]

https://doi.org/10.1021/acsnanoscienceau.2c00042
ACS Nanosci. Au 2023, 3, 94–102

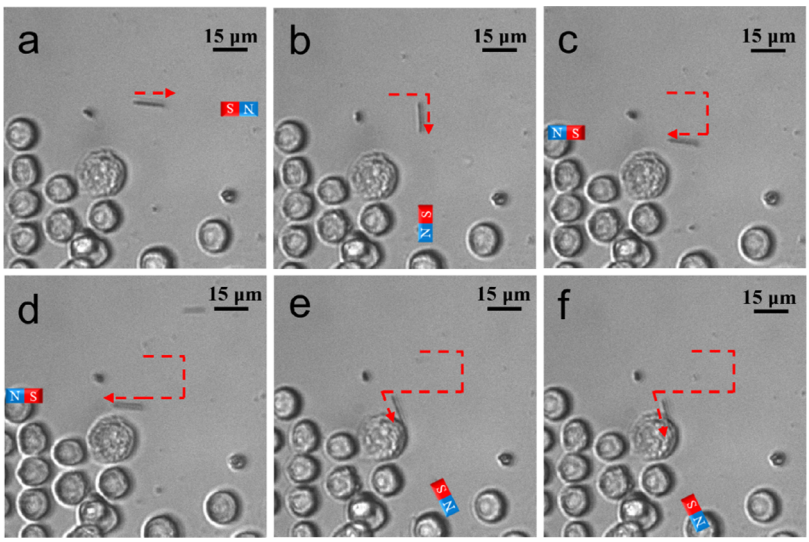

Figure 5. Diagram of the CNC/Fe_3O_4 @DOX nanomotor targeting the Hela cells' movement process (the red dashed line is the motion track).

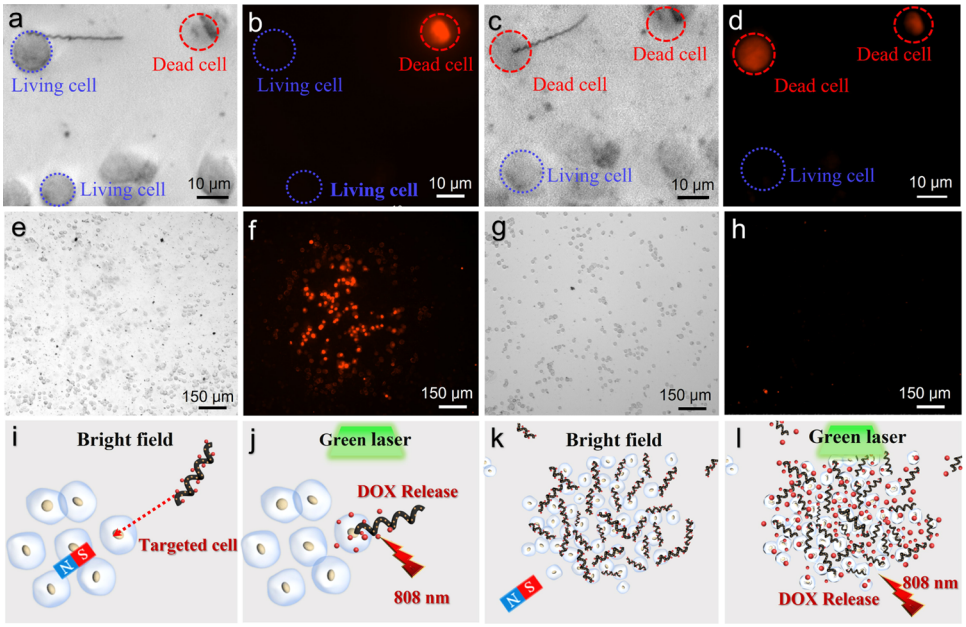

Figure 6. Comparison of bright-field images and fluorescence images of single CNCs/Fe_3O_4@DOX nanomotors targeting an individual target HeLa cell (a, b) before NIR irradiation at a wavelength of 808 nm and (c, d) after 180 s irradiation. A comparison of bright-field images and fluorescence images of clustered CNCs/Fe_3O_4@DOX nanomotors targeting a group of target cells. (e, f) HeLa cell solution mixed with CNCs/Fe_3O_4@DOX nanomotors and left for 46 min and (g, h) pure HeLa cell solution left for the same time. A schematic diagram of CNCs/Fe_3O_4@DOX nanomotors targeting HeLa cells for drug delivery: (i, j) single nanomotor targets a single HeLa cell and (k, l) population nanomotors target clustered target cells.

CONCLUSIONS

We have efficiently produced magnetically driven drug-loaded carbon nanomotors that effectively achieve cancer cell killing under irradiation of NIR light. For the first time, the functionalized CNC/Fe_3O_4 nanomotors were effectively prepared by combining microwave heating and CVD technology through a set of low-cost and easy-to-operate procedures. CNC/Fe_3O_4 was used as a carrier for drug delivery, and DOX was successfully modified on the surface of nanomotors by $\pi-\pi$ stacking, resulting in the fabrication of drug-loaded CNC/Fe_3O_4@DOX nanomotors. The position, direction, and speed of the nanomotor can be controlled remotely and precisely by optimally modulating the external magnetic field parameters.

CNC/Fe_3O_4 @DOX nanomotors could successfully target a single HeLa cell. Under short-term (~180 s) irradiation with NIR light, DOX was locally released in the targeted cells and facilitated the faster killing of the targeted HeLa cells. Such functionalized drug-delivery nanomotors can be controlled individually or in clusters to perform multiple tasks. The magnetically driven helical carbon-based nanomotor with good biocompatibility not only serves as an efficient drug carrier but also enables targeted drug delivery and potentially precision therapy. In summary, the efficient preparation method and innovative application of the carbon-based helical nanomotors in drug delivery are beneficial to future industrial production and lays the foundation for the wide application in the field of biomedicine.

https://doi.org/10.1021/acsnanoscienceau.2c00042
ACS Nanosci. Au 2023, 3, 94−102

■ ASSOCIATED CONTENT

Supporting Information

The Supporting Information is available free of charge at https://pubs.acs.org/doi/10.1021/acsnanoscienceau.2c00042.

CNCs/Fe_3O_4 nanomotors exhibiting linear motion behavior under magnetic field control (MP4)

CNCs/Fe_3O_4 nanomotors exhibiting horizontal direction control motion behavior under magnetic field control (MP4)

CNCs/Fe_3O_4 nanomotors exhibiting vertical direction control motion behavior under magnetic field control (MP4)

CNCs/Fe_3O_4 nanomotors exhibiting motion behavior in an AC magnetic field under magnetic field control (MP4)

■ AUTHOR INFORMATION

Corresponding Authors

Xing Ma − *School of Materials Science and Engineering, Harbin Institute of Technology (Shenzhen), Shenzhen 518055 Guangdong, China; Sauvage Laboratory for Smart Materials, Harbin Institute of Technology (Shenzhen), Shenzhen 518055 Guangdong, China;* orcid.org/0000-0002-2248-4806; Email: maxing@hit.edu.cn

Guo Ping Wang − *College of Electronics and Information Engineering, Shenzhen University, Shenzhen 518060, China*; Email: gpwang@szu.edu.cn

Authors

Yanming Sun − *College of Electronics and Information Engineering, Shenzhen University, Shenzhen 518060, China;* orcid.org/0000-0001-6898-8199

Renjie Pan − *College of Electronics and Information Engineering, Shenzhen University, Shenzhen 518060, China*

Yuduo Chen − *School of Materials Science and Engineering, Harbin Institute of Technology (Shenzhen), Shenzhen 518055 Guangdong, China; Sauvage Laboratory for Smart Materials, Harbin Institute of Technology (Shenzhen), Shenzhen 518055 Guangdong, China*

Yong Wang − *School of Materials Science and Engineering, Harbin Institute of Technology (Shenzhen), Shenzhen 518055 Guangdong, China; Sauvage Laboratory for Smart Materials, Harbin Institute of Technology (Shenzhen), Shenzhen 518055 Guangdong, China*

Lei Sun − *College of Electronics and Information Engineering, Shenzhen University, Shenzhen 518060, China*

Neng Wang − *College of Electronics and Information Engineering, Shenzhen University, Shenzhen 518060, China*

Complete contact information is available at: https://pubs.acs.org/10.1021/acsnanoscienceau.2c00042

Author Contributions

CRediT: **Yanming Sun** funding acquisition (lead), supervision (equal), writing-original draft (lead), writing-review & editing (lead); **Renjie Pan** investigation (equal), writing-original draft (equal); **Lei Sun** data curation (supporting), investigation (supporting), methodology (supporting).

Funding

The authors acknowledge financial support from the National Natural Science Foundation of China with Nos. 51908366, 11734012, 12074267, and 12174265; the Guangdong Natural Science Funds Grant with No. 2021A1515012069; the Shenzhen Science and Technology Program with Nos. JCYJ20200109113408066 and KQTD20170809110344233; and the Guangdong Rural Science and Technology Commissioner Project with No. KTP20200226.

Notes

The authors declare no competing financial interest.

■ ACKNOWLEDGMENTS

This work was financially supported by the National Natural Science Foundation of China (51908366, 11734012, 12074267, and 12174265), the Guangdong Natural Science Funds Grant (2021A1515012069), the Special Project for Research and Development in Key Areas of Guangdong Province (2020B010190001), the Shenzhen Science and Technology Program (JCYJ20200109113408066, KQTD20170809110344233), and the Guangdong Rural Science and Technology Commissioner Project (KTP20200226). The authors wish to acknowledge the assistance on HRTEM observation received from the Electron Microscope Center of Shenzhen University.

■ REFERENCES

(1) Enblad, M.; Birgisson, H.; Ekbom, A.; Sandin, F.; Graf, W. Increased incidence of bowel cancer after non-surgical treatment of appendicitis. *Eur. J. Surg. Oncol.* **2017**, *43*, 2067−2075.

(2) Wolf, B.; Ganzer, R.; Stolzenburg, J.-U.; Hentschel, B.; Horn, L.-C.; Höckel, M. Extended mesometrial resection (EMMR): Surgical approach to the treatment of locally advanced cervical cancer based on the theory of ontogenetic cancer fields. *Gynecol. Oncol.* **2017**, *146*, 292−298.

(3) Trimbos, J. B. Surgical treatment of early-stage ovarian cancer. *Best Pract. Res. Clin. Obstet. Gynaecol.* **2017**, *41*, 60−70.

(4) Chen, Y.; Wu, X.; Xian, X.; Zhang, Y.; Gong, N.; Qin, H.; Zhang, M. Adherence to oral chemotherapy among colorectal cancer patients: A longitudinal study. *Eur. J. Oncol. Nurs.* **2020**, *48*, No. 101822.

(5) Margalit, O.; Mamtani, R.; Lawrence, Y. R.; Yang, Y.-X.; Reiss, K. A.; Golan, T.; Halpern, N.; Aderka, D.; Giantonio, B.; Shacham-Shmueli, E.; Boursi, B. Postoperative Radiation for Pathologic Stage T4 Colon Cancers Receiving Adjuvant Chemotherapy. *Clin. Colorectal Cancer* **2019**, *18*, 226−230.

(6) Liontos, M.; Kaparelou, M.; Karofylakis, E.; Kavatha, D.; Mentis, A.; Zagouri, F.; Terpos, E.; Dimopoulos, M.-A. Chemotherapy resumption in ovarian cancer patient diagnosed with COVID-19. *Gynecol. Oncol. Rep.* **2020**, *33*, No. 100615.

(7) Dzierma, Y.; Minko, P.; Ziegenhain, F.; Bell, K.; Buecker, A.; Rübe, C.; Jagoda, P. Abdomin imaging dose in radiology and radiotherapy-Phantom point dose measurements, effective dose and secondary cancer risk. *Phys. Med.* **2017**, *43*, 49−56.

(8) Raby, S. E. M.; Choudhury, A. Radiotherapy for High-grade T1 Bladder Cancer. *Eur. Urol. Focus* **2018**, *4*, 506−508.

(9) Kaanders, J. H.; van den Bosch, S.; Dijkema, T.; et al. Advances in cancer imaging require renewed radiotherapy dose and target volume concepts. *Radiother. Oncol.* **2020**, *148*, 140−142.

(10) Lakshmi, B. A.; Kim, S. Current and emerging applications of nanostructured metal−organic frameworks in cancer-targeted theranostics. *Mater. Sci. Eng.: C* **2019**, *105*, No. 110091.

(11) Agrahari, V.; Agrahari, V.; Chou, M.-L.; Chew, C. H.; Noll, J.; Burnouf, T. Thierry Burnouf Intelligent micro-/nanorobots as drug and cell carrier devices for biomedical therapeutic advancement: Promising development opportunities and translational challenges. *Biomaterials* **2020**, *260*, No. 120163.

(12) Klumpp, S.; Lefèvre, C. T.; Bennet, M.; Faivre, D. Swimming with magnets: From biological organisms to synthetic devices. *Phys. Rep.* **2019**, *789*, 1−54.

(13) Goldstein, R. E. Green algae as model organisms for biological fluid dynamics. *Annu. Rev. Fluid Mech.* **2015**, *47*, 343−375.
(14) Alvarez, L.; Friedrich, B. M.; Gompper, G.; Kaupp, U. B. The computational sperm cell. *Trends Cell Biol.* **2014**, *24*, 198−207.
(15) Wu, Z.; Lin, X.; Wu, Y.; et al. Near-Infrared Light-Triggered "On/Off" Motion of Polymer Multilayer Rockets. *ACS Nano* **2014**, *8*, 6097−6105.
(16) Xie, S.; Xia, T.; Li, S.; Mo, C.; Chen, M.; Li, X. Bacteria-propelled microrockets to promote the tumor accumulation and intracellular drug uptake. *Chem. Eng. J.* **2020**, *392*, No. 123786.
(17) Xing, Y.; Zhou, M.; Du, X.; Li, X.; Li, J.; Xu, T.; Zhang, X. Hollow mesoporous carbon@Pt Janus nanomotors with dual response of H2O2 and near-infrared light for active cargo delivery. *Appl. Mater. Today* **2019**, *17*, 85−91.
(18) Chen, Z.; Xia, T.; Zhang, Z.; Xie, S.; Wang, T.; Li, X. Enzyme-powered Janus nanomotors launched from intratumoral depots to address drug delivery barriers. *Chem. Eng. J.* **2019**, *375*, No. 122109.
(19) Zhou, X.; Huang, X.; Wang, B.; Tan, L.; Zhang, Y.; Jiao, Y. Light/gas cascade-propelled Janus micromotors that actively overcome sequential and multi-staged biological barriers for precise drug delivery. *Chem. Eng. J.* **2021**, *408*, No. 127897.
(20) Srivastava, S. K.; Yadav, V. G. Bionic Manufacturing: Towards Cyborg Cells and Sentient Microbots. *Trends Biotechnol.* **2018**, *36*, 483−487.
(21) Ma, J.; Bai, W.; Zheng, J. A novel self-cleaning electrochemical biosensor integrating copper porphyrin-derived metal-organic framework nanofilms, G-quadruplex, and DNA nanomotors for achieving cyclic detection of lead ions. *Biosens. Bioelectron.* **2022**, *197*, No. 113801.
(22) Sharifi, M.; Hasan, A.; Attar, F.; Taghizadeh, A.; Falahati, M. Development of point-of-care nanobiosensors for breast cancers diagnosis. *Talanta* **2020**, *217*, No. 121091.
(23) Gao, W.; de Ávila, B. E.-F.; Zhang, L.; Wang, J. Targeting and isolation of cancer cells using micro/nanomotors. *Adv. Drug Delivery Rev.* **2018**, *125*, 94−101.
(24) Nguyen, H. V.; Faivre, V. Targeted drug delivery therapies inspired by natural taxes. *J. Controlled Release* **2020**, *322*, 439−456.
(25) Wang, Z.; Wang, S.; Liu, K.; Fu, D.; Ye, Y.; Gao, J.; Liu, L.; Wilson, D. A.; Tu, Y.; Peng, F. Water powered and anti-CD3 loaded mg micromotor for t cell activation. *Appl. Mater. Today* **2020**, *21*, No. 100839.
(26) Yang, R.; Song, B.; Sun, Z.; Chiu Lai, K. W.; Man Fung, C. K.; Patterson, K. C.; Seiffert-Sinha, K.; Sinha, A. A.; Xi, N. Cellular level robotic surgery: Nanodissection of intermediate filaments in live keratinocytes. *Nanomed.: Nanotechnol., Biol. Med.* **2015**, *11*, 137−145.
(27) Xu, J.; Cheng, X.; Chen, F.; Li, W.; Xiao, X.; Lai, P.; Xu, G.; Xu, L.; Pan, Y. Fabrication of multifunctional polydopamine-coated gold nanobones for PA/CT imaging and enhanced synergistic chemo-photothermal therapy. *J. Mater. Sci. Technol.* **2021**, *63*, 97−105.
(28) Rosli, N. F.; Mayorga-Martinez, C. C.; Fisher, A. C.; Alduhaish, O.; Webster, R. D.; Pumera, M. Arsenene nanomotors as anticancer drug carrier. *Appl. Mater. Today* **2020**, *21*, No. 100819.
(29) Li, X.; Sun, Y.-M.; Zhang, Z.-Y.; Feng, N.-X.; Song, H.; Liu, Y.-L.; Hai, L.; Cao, J.-M.; Wang, G. P. Visible light-driven multi-motion modes CNC/TiO2 nanomotors for highly efficient degradation of emerging contaminants. *Carbon* **2019**, *155*, 195−203.
(30) Dong, R. F.; Zhang, Q. L.; Gao, W.; Pei, A.; Ren, B. Highly efficient light-driven TiO2-Au Janus micromotors. *ACS Nano* **2016**, *10*, 839−844.
(31) Zhang, Y.; Lu, H.; Yan, B. Determination of urinary N-acetylneuraminic acid for early diagnosis of lung cancer by a boric acid covalently functionalized lanthanide MOFs and its intelligent visual molecular robot application. *Sens. Actuators, B* **2021**, *349*, No. 130736.
(32) Li, R.; Liu, J.; Zheng, X.; Peng, Q. Achieve 100% transmission via grafting hydroxyl groups on CNT nanomotors. *Curr. Appl. Phys.* **2021**, *29*, 59−65.
(33) Pei, C.; Wei, L.; Qin, Z.; Yu, H.; Zhu, J.-H.; Xing, F. Behavior and design of nano/micro-scale carbon modified multifunctional cementitious composites. *Constr. Build. Mater.* **2022**, *314*, No. 125506.
(34) Xu, P.; Yu, Y.; Li, T.; Chen, H.; Wang, Q.; Wang, M.; Wan, M.; Mao, C. Near-infrared-driven fluorescent nanomotors for detection of circulating tumor cells in whole blood. *Anal. Chim. Acta* **2020**, *1129*, 60−68.
(35) Dhar, P.; Narendren, S.; Gaur, S. S.; Sharma, S.; Kumar, A.; Katiyar, V. Self-propelled cellulose nanocrystal based catalytic nanomotors for targeted hyperthermia and pollutant remediation applications. *Int. J. Biol. Macromol.* **2020**, *158*, 1020−1036.
(36) Wang, W.; Duan, W. T.; Sen, A.; Mallouk, T. E. Catalytically powered dynamic assembly of rod-shaped nanomotors and passive tracer particles. *Proc. Natl. Acad. Sci. U.S.A.* **2013**, *110*, 17744−17749.
(37) Song, K.; Mohseni, M.; Taghipour, F. Mechanisms investigation on bacterial inactivation through combinations of UV wavelengths. *Water Res.* **2019**, *163*, No. 114875.
(38) Ren, L.; Nama, N.; McNeill, J. M.; Soto, F.; Yan, Z.; Liu, W.; Wang, W.; Wang, J.; Mallouk, T. E. 3D steerable, acoustically powered microswimmers for single-particle manipulation. *Sci. Adv.* **2019**, *5*, No. eaax3084.
(39) Zhao, Y.; Zuo, X.; Guo, Y.; Huang, H.; Zhang, H.; Wang, T.; Wen, N.; Chen, H.; Cong, T.; Muhammad, J.; Yang, X.; Wang, X.; Fan, Z.; Pan, L. Structural Engineering of Hierarchical Aerogels Comprised of Multi-dimensional Gradient Carbon Nanoarchitectures for Highly Efficient Microwave Absorption. *Nano-Micro Lett.* **2021**, *13*, No. 144.
(40) Khasraghi, S. S.; Shojaei, A.; Sundararaj, U. Highly biocompatible multifunctional hybrid nanoparticles based on Fe3O4 decorated nanodiamond with superior superparamagnetic behaviors and photoluminescent properties. *Mater. Sci. Eng.: C* **2020**, *114*, No. 110993.
(41) Gupta, A. K.; Gupta, M. Synthesis and surface engineering of iron oxide nanoparticles for biomedical applications. *Biomaterials* **2005**, *26*, 3995−4021.
(42) Schwertmann, U.; Cornell, R. M. *Iron Oxides in the Laboratory: Preparation and Characterization*; VCH: Weinheim, Cambridge, 1991.
(43) Cotin, G.; Piant, S.; Mertz, D.; Felder-Flesch, D.; Begin-Colin, S. *Iron Oxide Nanoparticles for Biomedical Applications: Synthesis, Functionalization, and Application*; Mahmoudi, M.; Laurent, S., Eds.; Elsevier, 2018; Chapter 2, pp 43−88.
(44) Zhao, Y.; Wang, J.; Huang, H.; Cong, T.; Yang, S.; Chen, H.; Qin, J.; Usman, M.; Fan, Z.; Pan, L. Growth of carbon nanocoils by porous α-Fe2O3/SnO2 catalyst and its buckypaper for high efficient adsorption. *Nano-Micro Lett.* **2020**, *12*, No. 23.
(45) Yaghoubi, A.; Ramazani, A. Anticancer DOX delivery system based on CNTs: Functionalization, targeting and novel technologies. *J. Controlled Release* **2020**, *327*, 198−224.
(46) Zhao, Y.; Zhang, H.; Yang, X.; Huang, H.; Zhao, G.; Cong, T.; Zuo, X.; fan, Z.; Yang, S.; Pan, L. In situ construction of hierarchical core−shell Fe3O4@C nanoparticles−helical carbon nanocoil hybrid composites for highly efficient electromagnetic wave absorption. *Carbon* **2021**, *171*, 395−408.
(47) Cao, Z.; Jiang, Z.; Cao, L.; Wang, Y.; Feng, C.; Huang, C.; Li, Y. Lattice expansion and oxygen vacancy of α-Fe2O3 during gas sensing. *Talanta* **2021**, *221*, No. 121616.
(48) Chen, M.; Shao, L. L.; Li, J. J.; Pei, W. J.; Chen, M. K.; Xie, X. H. One-step hydrothermal synthesis of hydrophilic Fe3O4/carbon composites and their application in removing toxic chemicals. *RSC Adv.* **2016**, *6*, 35228−35238.
(49) Ren, L.; Lin, H.; Meng, F.; Zhang, F. One-step solvothermal synthesis of Fe3O4@Carbon composites and their application in removing of Cr (VI) and Congo red. *Ceram. Int.* **2019**, *45*, 9646−9652.
(50) Xu, X.; Hou, S.; Wattanatorn, N.; Wang, F.; Yang, Q.; Zhao, C.; Yu, X.; Tseng, H. R.; Jonas, S. J.; Weiss, P. S. Precision-Guided Nanospears for Targeted and High-Throughput Intracellular Gene Delivery. *ACS Nano* **2018**, *12*, 4503−4511.
(51) Chen, Y.; Pan, R.; Wang, Y.; Guo, P.; Liu, X.; Ji, F.; Hu, J.; Yan, X.; Wang, G. P.; Zhang, L.; Sun, Y.; Ma, X. Carbon Helical Nanorobots Capable of Cell Membrane Penetration for Single Cell Targeted SERS Bio-Sensing and Photothermal Cancer Therapy. *Adv. Funct. Mater.* **2022**, *32*, No. 2200600.

https://doi.org/10.1021/acsnanoscienceau.2c00042
ACS Nanosci. Au 2023, 3, 94−102

(52) Chen, H.; Zhang, H.; Xu, T.; Yu, J. An overview of micronanoswarms for biomedical applications. *ACS Nano* **2021**, *15*, 15625−15644.

https://doi.org/10.1021/acsnanoscienceau.2c00042
ACS Nanosci. Au 2023, 3, 94−102